Bull Eng Geol Environ (2014) 73:747–758
DOI 10.1007/s10064-013-0543-y

ORIGINAL PAPER

A study of the effect of temperature on the structural strength of a clayey soil using a micropenetrometer

Kai Gu · Chaosheng Tang · Bin Shi · Jiaojiao Hong · Fei Jin

Received: 4 July 2013 / Accepted: 19 October 2013 / Published online: 16 November 2013

Abstract The effects of temperature on the behaviour of soils are of great concern in many geotechnical applications. This paper reports an experimental study that focused on the effect of temperature (between 20 and 50 °C) on the structural strength of a clayey soil using a modified micropenetrometer. Laboratory penetration tests using two penetration rates were conducted on highly overconsolidated specimens for which the degree of saturation (S_r) and dry density (ρ_d) were controlled. The results indicated that the penetration resistance (the total resistance, the friction and the end resistance) decreased with increasing temperature, suggesting that the structural strength of soil was softened by increasing the temperature. In addition, the rate of decrease in structural strength with increasing temperature was greater when the degrees of saturation was low and the dry density was high. Tests performed under cyclic heating and cooling revealed that subjecting the soil to this thermal cycling improves its structural strength. Moreover, increasing the rate of penetration caused higher penetration resistance, while its influence on the thermomechanical behaviour of the soil was only very slight.

Keywords Temperature effect · Structural strength · Penetration test · Unsaturated soil · Heating–cooling cycle · Thermomechanical behaviour

K. Gu · C. Tang · B. Shi (✉) · J. Hong
School of Earth Sciences and Engineering, Nanjing University, Nanjing 210093, China
e-mail: shibin@nju.edu.cn

K. Gu · F. Jin
Department of Engineering, University of Cambridge, Cambridge CB2 1PZ, UK

Introduction

The effects of temperature on the mechanical behaviour of soils are of great concern in many engineering contexts, such as road subgrade subjected to seasonal and daily cyclic changes in temperature, engineered barriers for nuclear waste disposal, the extraction of oil or geothermal energy, and urban applications of geothermal structures. Research carried out in this field over the last few decades, which has mainly focused on the changes in volume, shear strength, hydraulic features, and so on, with temperature, indicates that the effects of temperature on soils are quite complicated and often contradictory (Campanella and Mitchell 1968; Baldi et al. 1988; Hueckel and Borsetto 1990; Seneviratne and Carter 1993; Lingnau et al. 1996; Wiebe et al. 1998; Saix et al. 2000; Romero et al. 2001, 2003; Cekerevac and Laloui 2004; Villar and Lloret 2004; Bolzon and Schrefler 2005). Especially for unsaturated soils, changing the temperature alters the relative humidity in the voids, water adsorption forces, the surface tension at air–water interfaces, the soil structure, suction, the water retention capacity of the soil, and its dielectric constant. These factors are expected to interact in a complicated manner. Currently, the effects of temperature on the mechanical behaviour of soils are mainly investigated in a macroscopic way, using triaxial tests, direct shear tests, oedometer tests, etc. However, due to the complexity of soil material, the intrinsic mechanisms of the observed macrothermomechanical behaviour are not yet well understood. Generally, the mechanical characteristics of soil greatly depend on the shape, size, internal structure and strength of the aggregates that comprise it (Becher 1998; Mitchell and Soga 2005), but few detailed studies have explored the effects of temperature on the structural strength of soil aggregates in the lab.

The cone penetration test is widely considered to be an easy, rapid and relatively economical method to investigate soil strength parameters (Lunne et al. 1976; Elbanna and Witney 1987; Low et al. 2010; Shin and Kim 2011). Nevertheless, in field tests, the apparatus needed to study the soil strength is large, and it is not possible to predict the structural strength of soil based on microscopic observations. Here, the structural strength of soil can be defined as the referenced magnitude of intrusion force that must be imparted by a probe in order for it to pass through a microstructural unit of the soil. Shi et al. (2005) developed a micropenetrometer (SMP-1) that employed a probe with a very small diameter (1 mm). It was demonstrated that the SMP-1 can be used to determine the structural strength of soil aggregates (Liu et al. 2006).

In the work described in the present paper, in order to better understand the effect of temperature on the structural strength of soil, a series of penetration tests were conducted under controlled-temperature conditions (in the range 20–50 °C). The influences of thermal (heating–cooling) cycling, the degree of saturation, the dry density, and the penetration rate on the thermomechanical behaviour of soil was investigated and is discussed below.

Materials and methods

Soil

The laboratory tests were performed on a natural high-liquid-limit clayey soil (CH) from the Pukou District of Nanjing. The physical properties of the soil are summarised in Table 1. The mineralogical composition of the clay component was analysed by X-ray diffraction, which showed that the soil contained approximately 17.9 % montmorillonite, 73.6 % illite and 8.5 % kaolinite.

Apparatus

A schematic of SMP-1 is presented in Fig. 1. Generally, when a cylindrical probe penetrates into a soil vertically at a constant rate, the higher the soil strength, the greater the penetration resistance, and vice versa. The resistance caused by the soil matrix can be considered the reference magnitude of structural strength (Liu et al. 2006). This resistance consists of two components: the pressure required to expand a cavity in the soil, and the frictional resistance to the probe (Farrell and Greacen 1966). During the penetration process, the probe encounters both end resistance and peripheral friction (Fig. 2a), while it

Table 1 Physical properties of the clayey soil

Property	Value
Specific gravity	2.71
Liquid limit	76 %
Plastic limit	29 %
Plasticity index	47
Sand	24.4 %
Silt	33.6 %
Clay	42.0 %

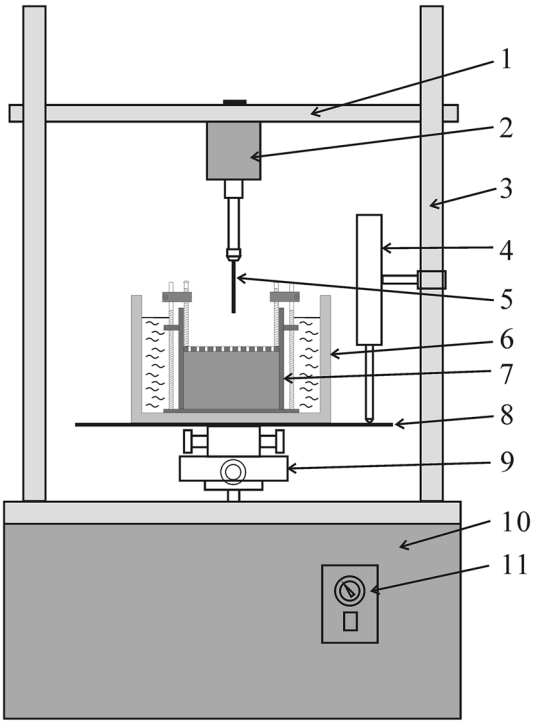

Fig. 1 Schematic of the modified SMP-1 apparatus: *1* crossbeam, *2* load cell, *3* vertical shaft, *4* displacement transducer, *5* probe, *6* water bath, *7* container and specimen, *8* loading disk, *9* traverse plate, *10* control box, *11* control panel

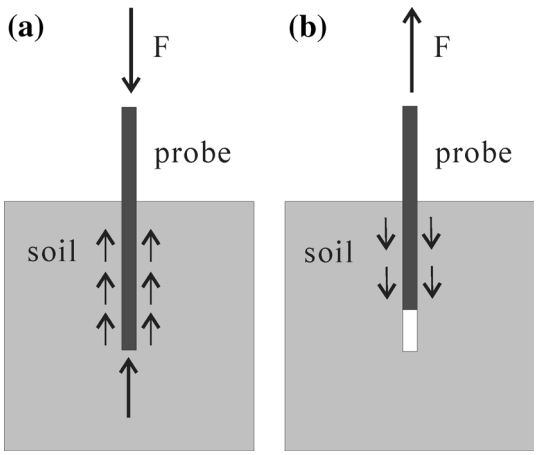

Fig. 2 Soil resistance to the probe during **a** the penetration and **b** the withdrawal of the probe

encounters only peripheral friction when it is withdrawn (Fig. 2b). Assuming that (1) the friction during penetration equals the friction during withdrawal, and (2) none of the soil accumulates on the end of the probe due to its small diameter (1 mm), the relationship between the end resistance and the corresponding penetration depth can be obtained by deducting the peripheral friction from the total penetration resistance at the corresponding depth. For SMP-1, penetration and withdrawal of the probe (5 in Fig. 1) are realised by lifting and lowering the traverse plate (9 in Fig. 1), respectively. The load cell (2 in Fig. 1) at the opposite end of the probe is used to measure the total resistance during penetration and the friction during withdrawal. The displacement transducer (4 in Fig. 1) is used to measure the penetration depth. A water bath (6 in Fig. 1) is also fixed onto the loading disk to control the temperature during tests.

Calibration

The measured data collected from the load cell and the displacement transducer were voltage signals. Therefore, calibration was carried out to obtain the calibration coefficients needed to transform the collected data into real resistance and displacement values. The linear relationships between the measured voltage signals and the real resistance and displacement values were as follows:

$$\mathrm{PR} = \mathrm{ER} \times 19.948 - 3.591, \quad R^2 = 1 \tag{1}$$

$$\mathrm{PD} = \mathrm{ED} \times 10.001 + 0.060, \quad R^2 = 1, \tag{2}$$

where PR is the penetration resistance that the probe encounters during the penetration process, ER is the voltage obtained in the resistance channel, PD is the displacement of the probe, and ED is the voltage obtained in the displacement channel.

Preparation of specimens

The air-dried soil was first ground up such that it could pass through a 2-mm sieve. Prior to preparation, the soil was oven dried at 105 °C for 24 h and then cooled to room temperature in a desiccator. Predetermined amounts of distilled water and soil were carefully mixed and cured in sealed plastic bags at room temperature for 24 h to achieve homogeneity. A steel container 105 mm in height and 99.2 mm in inner diameter was specially designed for the test. Figure 3a shows a schematic drawing of the container. Three long fixing bars (two visible in Fig. 3a) were used to fix the baseplate. The soil was then statically and hierarchically compacted into the container. The final dimensions of the specimen were 60 mm in height and 99.2 mm in diameter. In order to prevent moisture evaporation and unnecessary displacement during the test, a thin top cover (Fig. 3b) was placed on the specimen's surface and fixed by three short fixing bars. In the metal cover, a total of 97 small holes (3 mm in diameter) were drilled to allow penetration. The distance between neighboring holes was 8.2 mm, which was much larger than the diameter of the penetration probe (1 mm). The influence of the soil deformation caused by penetration on adjacent penetration points could therefore be ignored. Finally, all of the joints that could possibly allow water to pass through were sealed with silicon sealant. In total, 11 specimens with different ρ_d and S_r values were prepared. The details for each specimen are shown in Table 2.

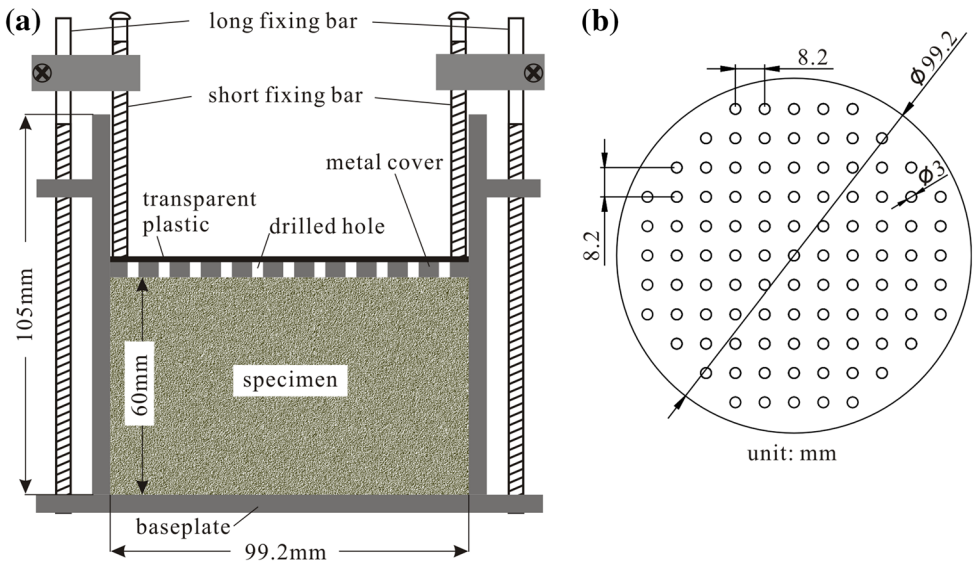

Fig. 3 Schematic diagram of the specimen container and its adjunct. **a** Profile of the container. **b** Top view of the top cover

Table 2 Physical properties of and penetration depths into the specimens

No.	ρ_d (g/cm^3)	S_r (%)	Penetration depth (mm)
S1	1.46	60	30
S2	1.46	70	40
S3	1.46	80	40
S4	1.46	90	40
S5	1.54	70	25
S6	1.54	80	40
S7	1.54	90	40
S8	1.62	80	40
S9	1.62	90	40
S10	1.46	70	35
S11	1.54	70	35

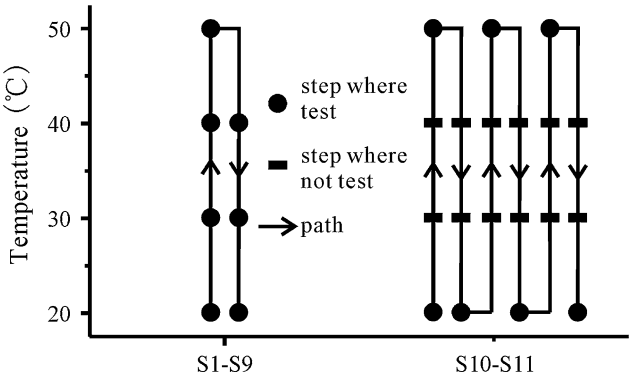

Fig. 4 Temperature paths applied to the specimens

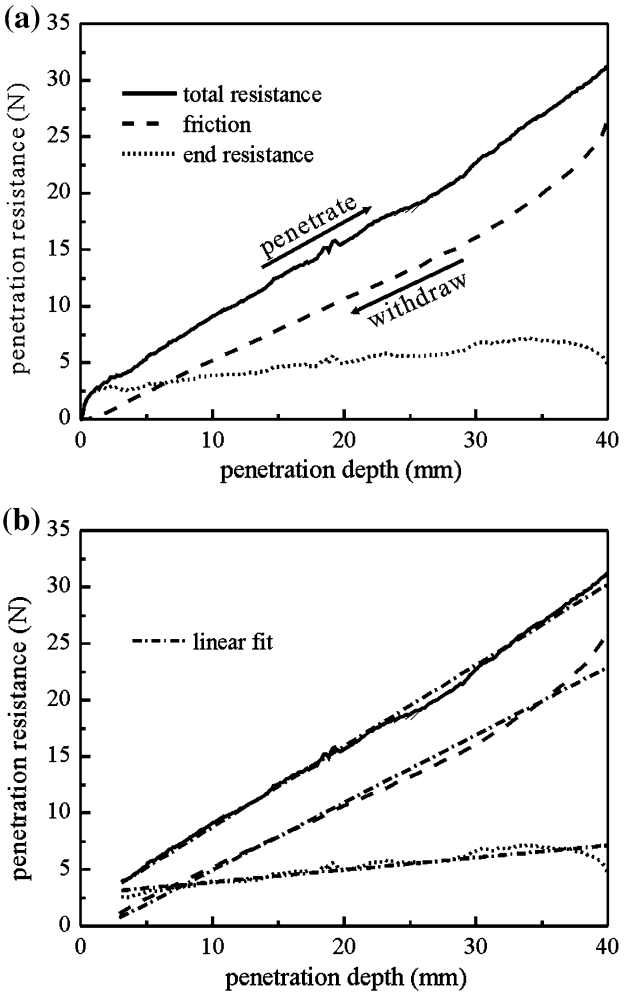

Fig. 5 Typical relationships between the resistance and the penetration depth. **a** Original curves. **b** Linear curve fits

Test program

A series of penetration tests were carried out on the prepared specimens at different temperatures. Figure 4 explains the temperature path applied to the specimens and the temperature steps at which tests were carried out. One heating–cooling cycle was applied in tests S1–S9, while three heating–cooling cycles were applied in tests S10 and S11. For each test, the initial temperature was maintained at 20 °C. The temperature was increased from 20 to 30, 40 and 50 °C step by step. During the subsequent cooling steps, the temperature was decreased from 50 to 40, 30 and 20 °C step by step. At each temperature step, the specimen was maintained in an oven for at least 16 h, making sure that the temperature inside the specimen was homogeneous. The specimen was then subjected to penetration tests. By applying a water bath, the temperature of each specimen was kept constant during the penetrations. After all of the penetrations had been performed at each temperature step, the specimens were again cured in the oven for another 16 h at the next temperature step.

In tests S1–S9, 13 parallel penetration tests were performed at each temperature step, of which ten were implemented at a constant penetration rate of 10 mm/min while the other three were carried out at a rate of 5 mm/min. In tests S10 and S11, seven parallel tests were carried out at a rate of 10 mm/min and temperatures of 20 and 50 °C. The penetration positions were carefully selected to reflect the structural strength of the specimen as accurately as possible. In order to reduce moisture evaporation, only one hole in the top cover was open for penetration; the others were sealed by adhesive tape during the test. The open hole was resealed afterwards. The water contents of small samples extracted at different depths were measured after all of the tests had been performed for each sample.

Resistance data and displacement signals were acquired by a computer, with the sampling interval set at 1 s. It should be noted that the probe occasionally became stuck during withdrawal due to the high structural strengths of

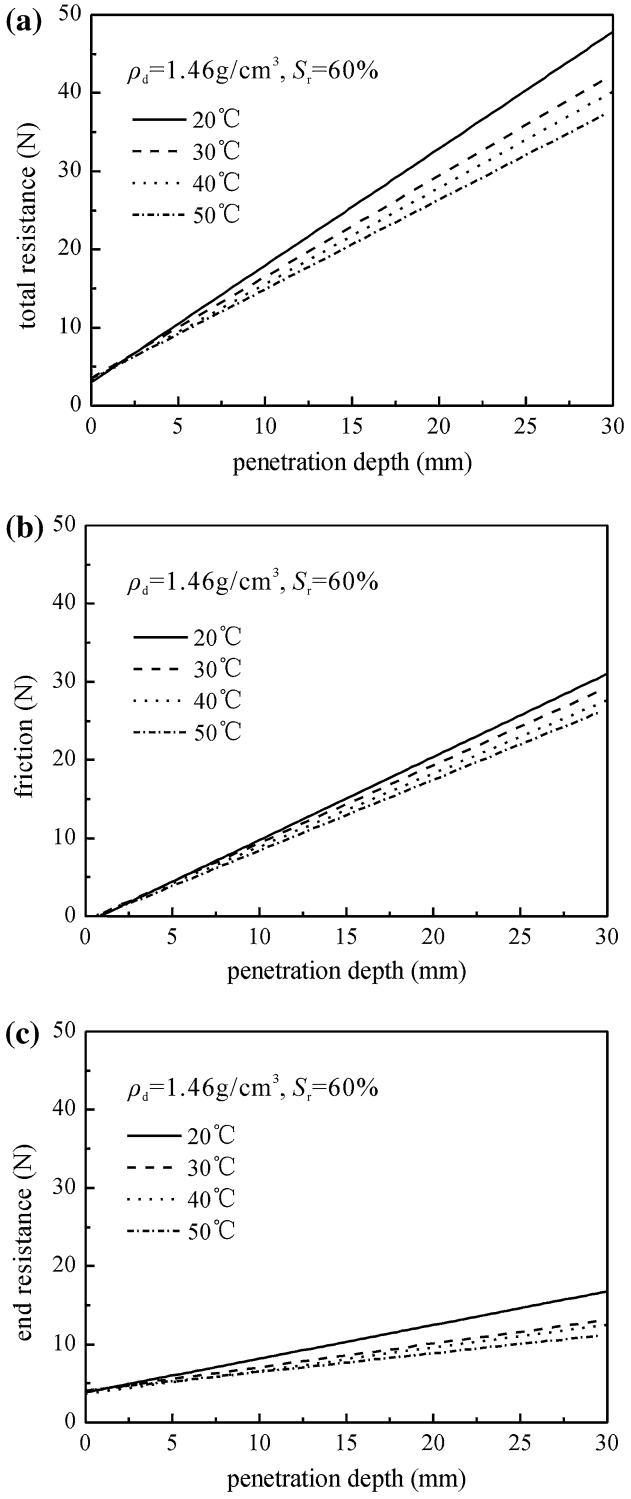

Fig. 6 Effect of temperature on the penetration resistance (plots show effects on **a** total resistance, **b** friction, **c** end resistance)

some specimens, so different penetration depths were tested on different specimens (Table 2). In this investigation, a total of 917 penetration tests were performed.

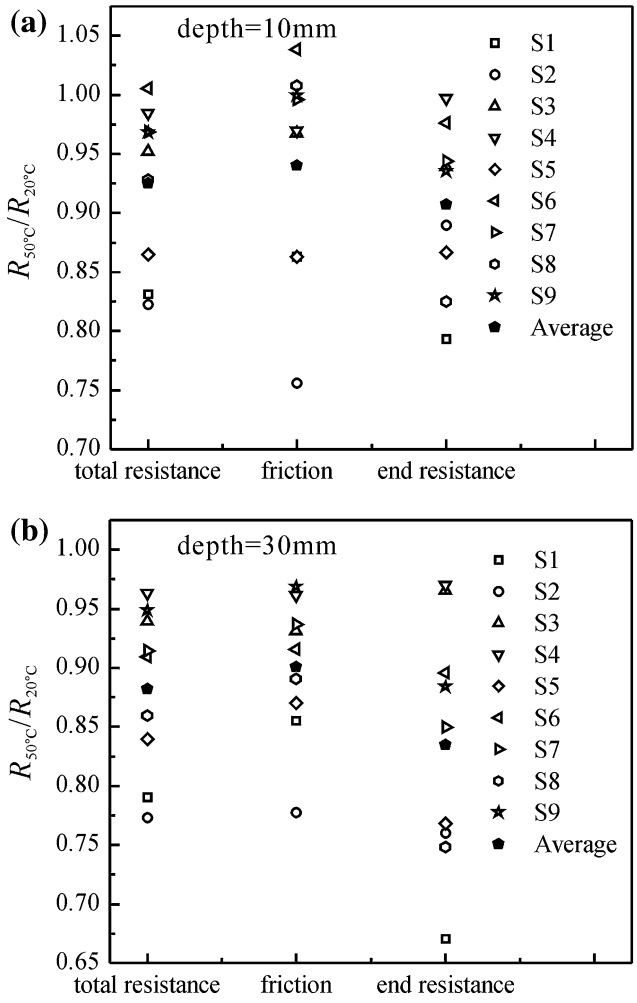

Fig. 7 Ratios of the resistance at 50 °C to the resistance at 20 °C at depths of **a** 10 mm and **b** 30 mm

Results

Penetration curves and linear curve fitting

Typical penetration curves, and the relationship between the penetration resistance and the penetration depth, are illustrated in Fig. 5a, where the friction curve is plotted based on the value measured during withdrawal, and the end resistance curve is plotted by deducting the friction from the measured total resistance during penetration. At the initial stage (i.e. when the penetration depth is less than 3 mm), the total resistance curve increases sharply due to the end resistance, while the friction is very small and can be ignored. After that, the total resistance and the friction increase linearly with the penetration depth. These two curves are smooth, indicating that the prepared specimen is highly homogeneous. To perform a detailed analysis of the obtained data, all three curves were subjected to linear

curve fitting (ignoring the data for the first 3 mm of depth; Fig. 5b), and the equations for the linear curve fits obtained were as follows:

$$\mathrm{PR} = a_1 \times \mathrm{PD} + b_1 \quad (3)$$

$$f = a_2 \times \mathrm{PD} + b_2 \quad (4)$$

$$\mathrm{ED} = a_3 \times \mathrm{PD} + b_3, \quad (5)$$

where PR is the penetration resistance, f is the friction, ED is the end resistance, PD is the penetration depth, a_1, a_2, a_3 are the slopes, and b_1, b_2, b_3 are the intercepts.

As mentioned in the "Test program" section, ten parallel penetration tests were performed at a penetration rate of 10 mm/min, and three at 5 mm/min. Hence, the slopes and intercepts of the linear curve fits at each test condition represent the mean values of the parallel fit results.

Effect of temperature on the structural strength

Figure 6 shows the variations in the total resistance, the friction and the end resistance of S1 ($\rho_d = 1.46$ g/cm^3, $S_r = 60$ %) with penetration depth at different temperatures (from 20 to 50 °C). As can be seen, the penetration resistance presents evident thermal softening behaviour. At a depth of 30 mm, elevating the temperature from 20 to 50 °C decreases the total resistance, the friction and the end resistance by 21, 14 and 33 %, respectively. The ratios of the penetration resistance at 50 °C to the resistance at 20 °C at depths of 10 and 30 mm are presented in Fig. 7. In general, the penetration resistances are reduced by increasing the temperature, although the ratios vary with the penetration depth. The average ratios of the resistances indicate that the end resistance is more temperature dependent than the peripheral friction.

Factors that influence the thermomechanical behaviour

Effect of thermal (heating–cooling) cycling

A single heating and cooling loop was applied to each of S1 to S9. Figure 8 illustrates the variation in the end resistance at a depth of 30 mm with cyclic changes in temperature. As expected, heating softens the soil, while cooling strengthens the soil. It is also found that the penetration resistance during the cooling path is higher than that during the heating process, suggesting that cyclic heating–cooling can improve the structural strength of soil. This was further confirmed by the tests on S10 and S11, which were subjected to three temperature cycles. The results are presented in Fig. 9. Note that the results for the

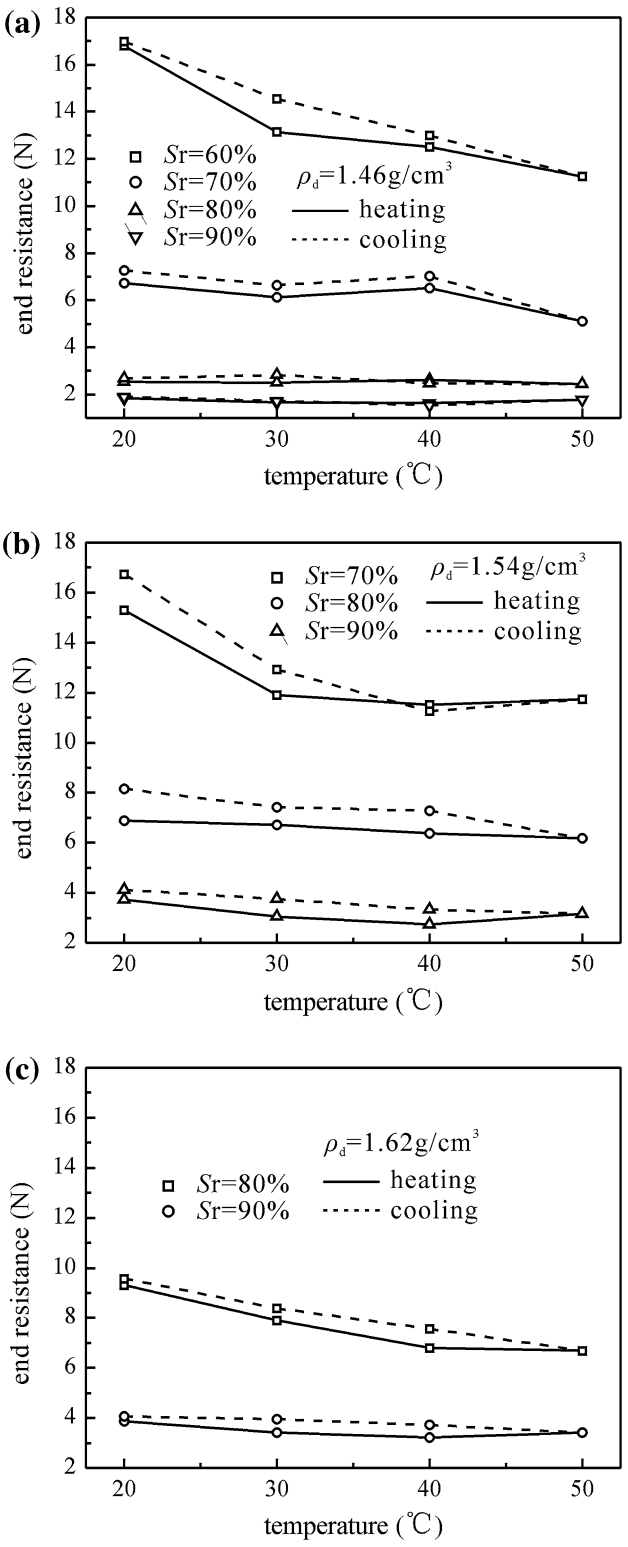

Fig. 8 Variation in the end resistance at 30 mm depth during a heating–cooling cycle: **a** ρ_d = 1.46 g/cm^3, **b** ρ_d = 1.54 g/cm^3, **c** ρ_d = 1.62 g/cm^3

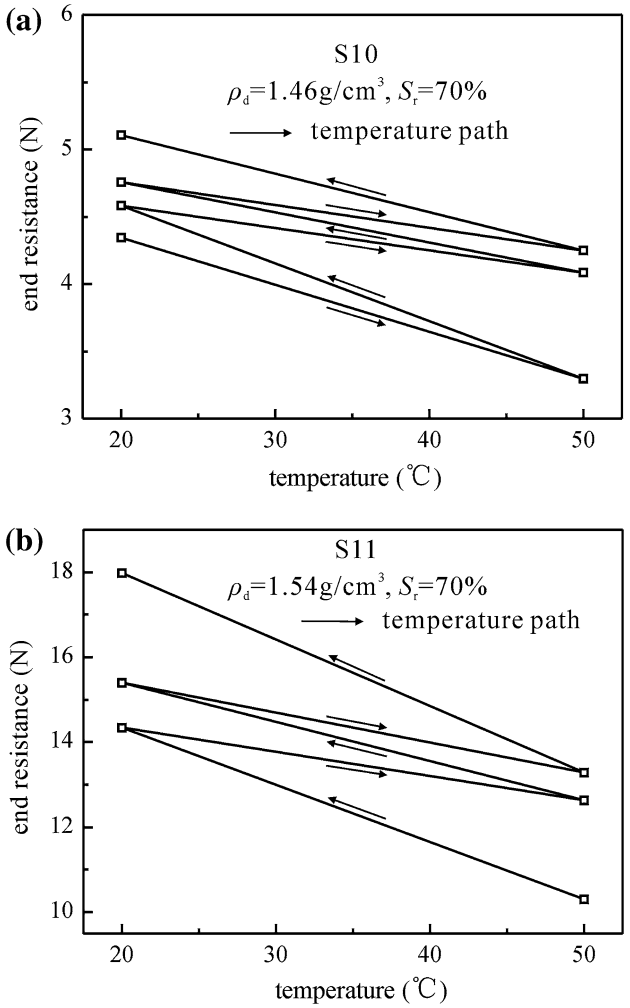

Fig. 9 Effect of thermal (heating–cooling) cycling on the end resistance (at 30 mm depth): **a** ρ_d = 1.46 g/cm^3, **b** ρ_d = 1.54 g/cm^3

first heating path for S11 were lost because of an equipment failure (Fig. 9b). A general trend can be observed: in each cycle, the end resistance measured during the heating path is lower than that measured during the cooling path, indicating that the structural strength of the soil is greater during the cooling path. On the other hand, it also can also be observed that there is no clear trend in the variation of the slope of the relationship between temperature and resistance during the thermal cycles according to Fig. 9.

Effect of the degree of saturation

The influence of S_r on the penetration resistance–temperature relationship was consistent across all specimens. A typical relationship for a group of specimens at the same ρ_d (1.46 g/cm^3) but different S_r values (60–90 %, S1, S2, S3, and S4) is shown in Fig. 10, which presents the total resistance, the friction and the end resistance at a depth of 30 mm. At an S_r of 60 %, the value of the total resistance

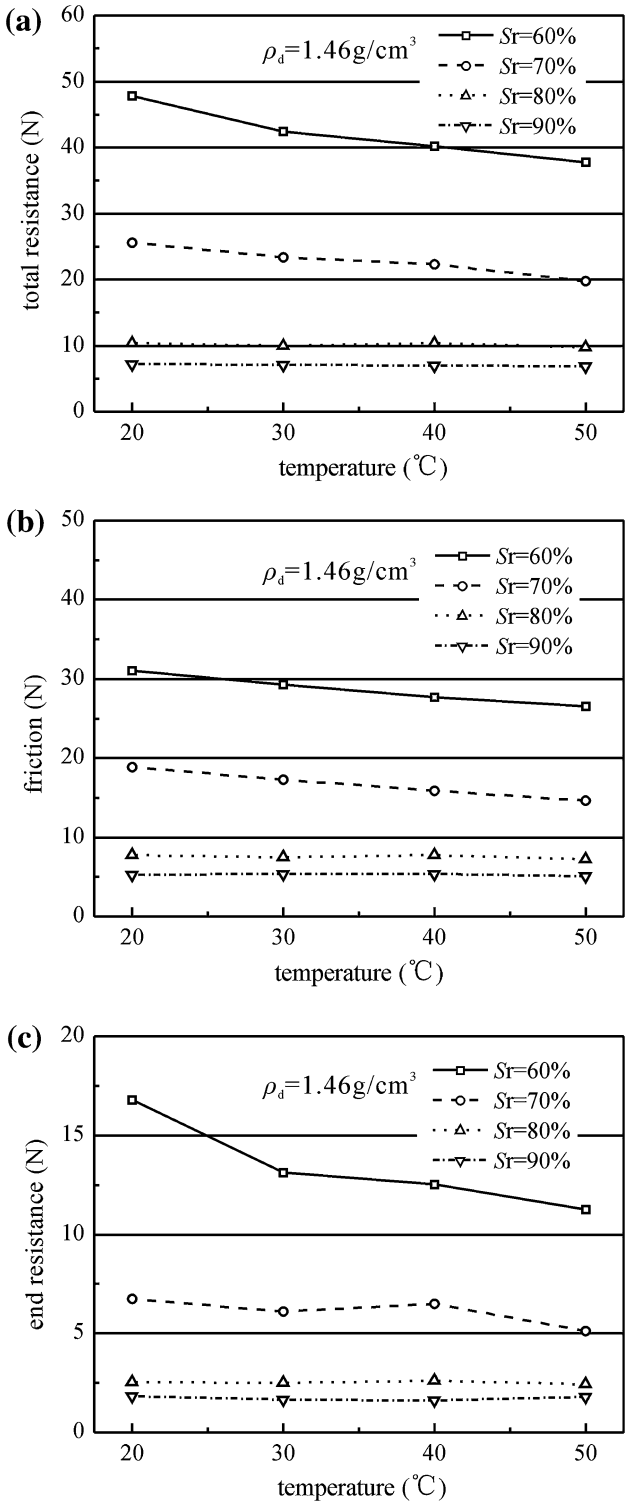

Fig. 10 Relationship between the temperature and the penetration resistance at a depth of 30 mm: **a** total resistance, **b** friction and **c** end resistance

decreases considerably with increasing temperature, at an approximate rate of −0.322 N/°C (Fig. 10a). However, this rate of decrease drops significantly with increasing S_r.

Table 3 Rates of variation in the resistance with increasing temperature at a depth of 30 mm

S_r (%)	Variation rate (N/°C)		
	Total resistance	Friction	End resistance
60	−0.322	−0.150	−0.172
70	−0.184	−0.140	−0.045
80	−0.015	−0.014	−0.002
90	−0.009	−0.007	−0.002

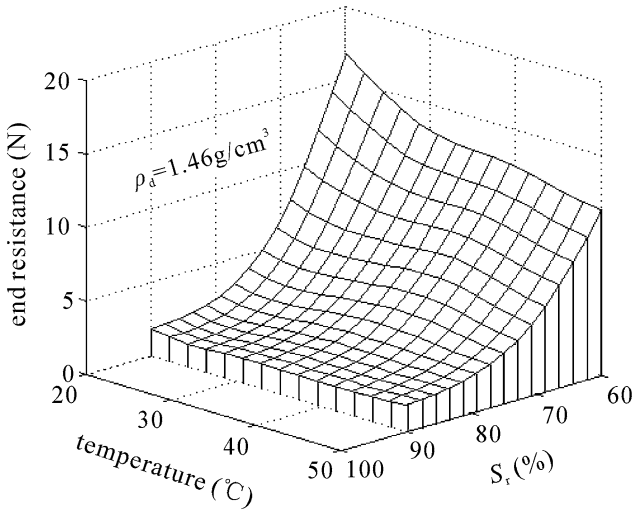

Fig. 11 Three-dimensional surface of the end resistance versus the degree of saturation and the temperature

Table 3 summarises the rates of variation in the total resistance, the friction and the end resistance with increasing temperature. At higher S_r values (i.e. 80, 90 %), the rate of decrease is close to zero. Hence, it can be concluded that thermal softening of the soil decreases with increasing S_r.

Three-dimensional surfaces of the end resistance versus degree of saturation and temperature for S1, S2, S3 and S4 are shown in Fig. 11. It is clear that the surface becomes steeper when S_r approaches 60 %, while it is approximately flat when the soil approaches saturation, indicating that the structural strength of soil with a low degree of saturation clearly varies with temperature, while soil with a high degree of saturation is relatively insensitive to temperature.

Effect of dry density

Figure 12 shows the relationship between the end resistance at 30 mm depth and temperature for specimens with the same S_r (80 %) but different ρ_d (1.46–1.62 g/cm^3, S3, S6 and S8). It can be seen that the effect of temperature on the end resistance varies with ρ_d. For the specimen with the lowest density (S3, ρ_d = 1.46 g/cm^3), the end resistance changes only slightly with temperature. As the dry density was increased, the dependence of the end resistance on the temperature became more evident. As is shown in Fig. 12, the rate of variation with temperature during the heating process was approximately −0.025 N/°C for 1.54 g/cm^3 and −0.090 N/°C for 1.62 g/cm^3, indicating that thermal softening of the soil is more significant in denser soils.

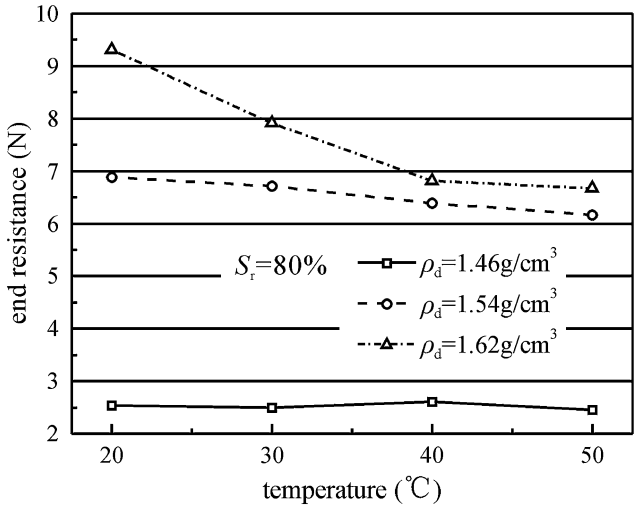

Fig. 12 Effect of dry density on the end resistance, S_r = 80 %

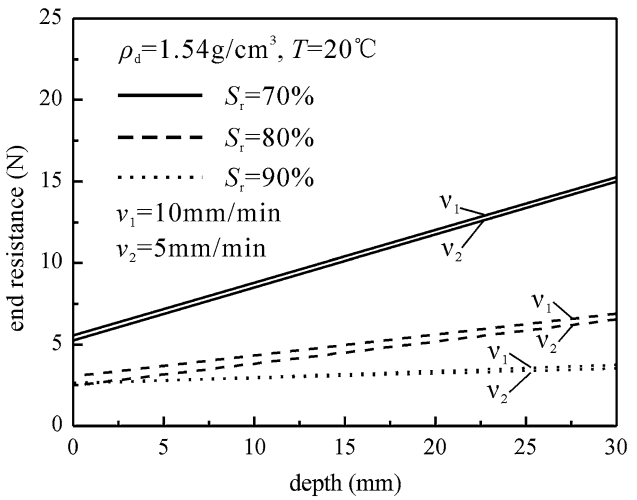

Fig. 13 Effect of penetration rate on the end resistance

Effect of penetration rate

Two different penetration rates, v_1 = 10 mm/min, and v_2 = 5 mm/min, were applied to tests S1–S9. Figure 13

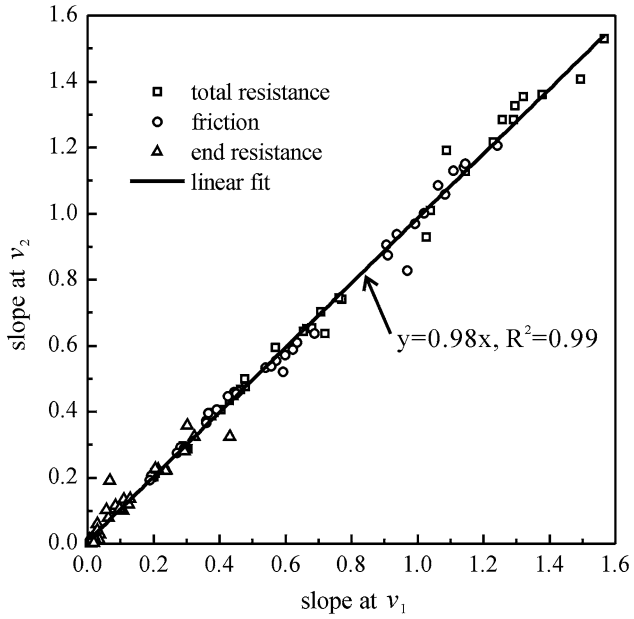

Fig. 14 Slope of the linear curve fits at v_1 versus the slope at v_2

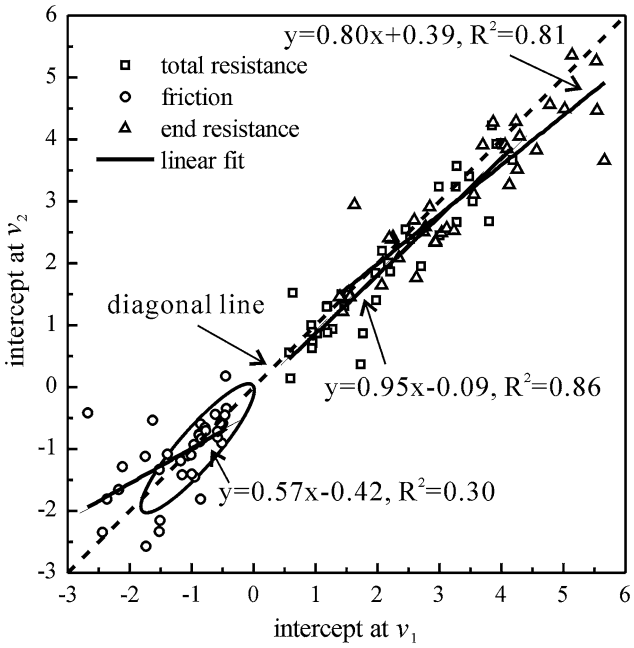

Fig. 15 Intercepts of the linear curve fits at v_1 versus the intercepts at v_2

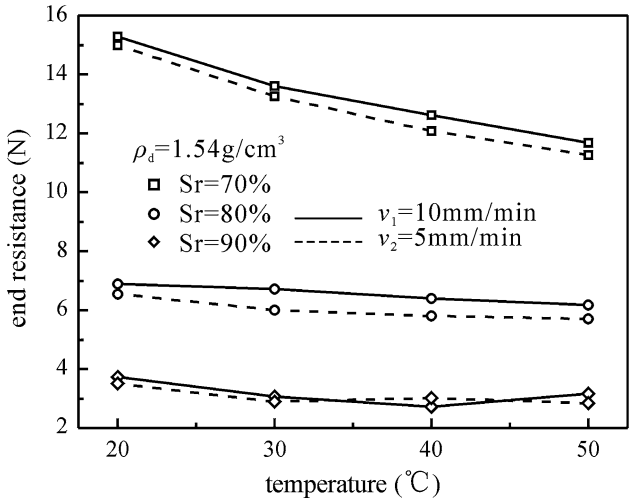

Fig. 16 Effect of penetration rate on the end resistance at different temperatures

illustrates a typical relationship between the end resistance and the penetration depth observed at different penetration rates while the temperature was kept constant. It was found that the end resistance is higher when the penetration rate is 10 mm/min. Moreover, the curves for the same specimen are approximately parallel, suggesting that the rate of increase of the resistance may be independent of the penetration rate. Upon plotting the slopes of the linear curve fits of resistance at different rates during the heating process for all of the tested samples except for S10 and S11 (Fig. 14, x-axis is the slope obtained at v_1 and y-axis is the slope obtained at v_2), no clear difference was observed between the slopes obtained at two rates, as the slope of the linear curve fit is extremely close to 1 ($y = 0.98x$, $R^2 = 0.99$). The intercepts, which represent the penetration resistance at the sample surface, are slightly higher when the rate is 10 mm/min, since the fit curves are below the diagonal line (Fig. 15). This trend is not clearly observed for the friction due to the scatter in the data, but the dominant points in the circle may suggest that the intercepts of the friction do not vary significantly with penetration rate. Figures 14 and 15 together reveal that the total and end resistances to penetration are high when the rate of penetration is high, while the variation in the peripheral friction with penetration rate was not significant.

On the other hand, thermal softening was observed to be irrelevant to the rate of penetration. As is shown in Fig. 16, the rates of decrease in the end resistance with temperature were essentially the same at different penetration rates.

Discussion

Thermal softening of soil structural strength

For all specimens investigated, it was found that increasing the temperature resulted in a softening of the structural strength of the soil. In general, increasing the temperature results in thermal expansion of the soil aggregates as well as the pore water, which reduces the strengths of these

components. Hence, the volume change induced by temperature is highly dependent on the overconsolidation ratio, OCR. It was observed that heating resulted in a volume increase at large OCR but a decrease at small OCR (Baldi et al. 1988; Towhata et al. 1993; Sultan et al. 2002; Abuel-Naga et al. 2007). In a thermomechanical model of saturated clays, Cui et al. (2000) described the expansion of soil constituents (soil particles and pore water) during heating, which explains the phenomenon of macroscopic thermal expansion under low stress.For unsaturated soils, Romero et al. (2005) reported that compacted FEBEX bentonite exhibited smaller final strains as the temperature was increased while the sample was placed under 0.5 MPa of vertical stress, while the trend for strain was not very clear when the vertical stress was 3 MPa. Tang et al. (2008) observed that the volumetric thermal behaviour was strongly affected by pressure and suction. They found that heating induced expansion under low pressure (0.1 MPa) and high suction (110 MPa), whereas it tended to induce contraction under high pressure (5 MPa) and low suction (9 MPa). Since vertical stress was not applied to the specimens in this study, the decrease in the end resistance was attributed to the softening of soil particles and contacts between aggregates resulting from the soil expansion induced by heating. In addition, the drop in resistance was also related to the increase in the intra-aggregate pore pressure with increasing temperature. Romero et al. (1999) investigated the morphology of the pores in unsaturated Boom clay and found that intra-aggregate water represented between 54 and 59 % of the total volume of water in soil in a low-porosity packing that was compacted at a dry unit weight of 16.7 kN m^{-3}, whereas it reduced to 28 and 38 % when it was in a high-porosity packing that was compacted at a dry unit weight of 13.7 kN m^{-3}. In contrast to the inter-aggregate water, quasi-immobile intra-aggregate water is barely affected by mechanical processes (Romero et al. 1999). It is reasonable to conclude that the pore pressure of intra-aggregate water increases with increasing temperature, which results in the decrease in the end resistance.

The decrease in the peripheral friction with temperature can be attributed to the effect of temperature on the rearrangement and rotation of soil particles as well as the matric suction. Tang et al. (2010) found that the interfacial friction was highly dependent on the resistance of the soil particles to rearrangement and rotation through single-fibre pull-out tests. Thermal softening of soil particles and contacts leads to lower resistance of particles to rearrangement and rotation along the probe's surface. Furthermore, the matric suction occurs due to the presence of capillary water between the soil particles and the probe surface. It was found that the capillary pressure decreases linearly with temperature due to the corresponding decrease in the kinematic viscosity of water (Gardner 1955; Grant and Salehzadeh 1996). Wiebe et al. (1998) and Haghighi et al. (2011) also observed that soil suction was lower at higher temperatures for specimens with the same void ratio and water content. The smaller matric suction that occurs at higher temperatures reduces the penetration resistance.

The effect of temperature on the structural strength is observed to vary with the S_r and ρ_d values of the specimens. The rate of decrease of the resistance with increasing temperature is higher at lower S_r and higher ρ_d. As pointed out by other researchers (Delage and Graham 1996), the soil structure and the pore size are highly dependent on the degree of saturation. At lower S_r values, the pores and soil aggregates are small, giving rise to high suction in the micropores within soil aggregates (Wiebe et al. 1998). This higher suction is more sensitive to changes in temperature. On the other hand, bulk water is preponderant in the inter-aggregate zone at higher S_r (Romero et al. 2001). The effects of temperature on the surface tension and the thickness of diffuse double layers are less significant because of the smaller suction involved and the more deformable and weaker soil particles present. The three-dimensional surface in Fig. 11 indicates that the structural strength of saturated soil may be independent of temperature because the surface is very flat when it approaches the saturated condition. The apparent effect of temperature on denser specimens can be attributed to more contacts between the soil particles and lower porosity.

Irreversible thermomechanical behaviour of the soil

Irreversible changes induced by temperature have been investigated by many authors, who have mainly focused on volumetric strains (Romero et al. 2005; Lloret and Villar 2007). However, our understanding of the effect of thermal (heating–cooling) cycling on structural strength is limited. According to Figs. 8 and 9, the structural strength of the soil increases with cyclic heating–cooling. The water contents of the samples measured after the test program was completed were no different from the initial water contents, indicating that the improvement in soil strength does not result from the loss of water from the samples. The increased penetration resistance can be explained by the accumulation of strain during the thermal cycles. Measurement of the axial thermal expansion coefficient of compacted bentonite under mechanically unconfined conditions, as performed by Romero et al. (2005), revealed that some axial strain was irreversible after the first heating–cooling cycle. Due to the thermal expansion of mineral particles and adsorbed water, there are some irreversible effects on the soil skeleton at low vertical stress. By contrast, it was observed by Uchaipichat and Khalili (2009)

that the specific volume of the soil was reduced by thermal loading and unloading with a net stress of 50 kPa, and the effect was more significant when the net stress was increased to 200 kPa, leading the authors to conclude that the volume change due to heating in highly overconsolidated soil took the form of an elastic dilation. Nevertheless, in the present study, the increase in penetration resistance indicates increasing internal stiffness after thermal cycling, but the variation of increment with cycling number is not clear yet. The end resistance at 20 °C increases by 0.24 N after the initial heating–cooling cycle, while it increases by 0.17 and 0.35 N in the following two cycles, respectively (Fig. 9a). Meanwhile, the end resistance at 50 °C increases by 0.79 and 0.16 N during the first two heating–cooling cycles. Irregular increases in internal stiffness with thermal cycling can be seen in Fig. 9b as well.

Conclusions

A series of tests were carried out using a micropenetrometer (SMP-1). Four temperature levels (20, 30, 40, 50 °C) and a specific number of temperature cycles were applied to identify the effects of temperature on the penetration resistance. A series of highly overconsolidated clayey soil specimens with different dry densities and degrees of saturation were tested at two different rates of penetration (10 and 5 min/mm). Based on the results obtained, the following conclusions can be drawn.

1. The effect of temperature on the structural strength of the soil was clearly reflected in the results of the penetration tests performed using the SMP-1 micropenetrometer.
2. In general, for the type of soil studied, increasing the temperature reduced the structural strength of the soil, and evident thermal softening behaviour was observed.
3. Applying heating and cooling cycles improved the soil strength, indicating that some of the thermomechanical behaviour is irreversible.
4. The effect of temperature on the structural strength is observed to vary with the degree of saturation (S_r) and the dry density (ρ_d) of the specimen. The rate of decrease in the resistance with increasing temperature is higher at low S_r and high ρ_d.
5. The structural strength of the soil, as obtained using penetration tests, increases with an increasing penetration rate, but the thermomechanical behaviour of the soil is not affected by the penetration rate.

Acknowledgments The authors wish to acknowledge the financial support provided by the Key Project of the Natural Science Foundation of China (nos. 40730739, 41230636), the Scientific Research Foundation of the Graduate School of Nanjing University (no. 2012CL11), the National Basic Research Program of China (no. 2011CB710605) and the National Natural Science Foundation of China (nos. 41072211, 41072210, 41322019).

References

Abuel-Naga HM, Bergado DT, Bouazza A (2007) Thermally induced volume change and excess pore water pressure of soft Bangkok clay. Eng Geol 89:144–154. doi:10.1016/j.enggeo.2006.10.002

Baldi G, Hueckel T, Pellegrini R (1988) Thermal volume changes of the mineral–water system in low-porosity clay soils. Can Geotech J 25:807–825

Becher H (1998) Resistances to penetration of aggregates from loess-derived topsoils at different soil water tensions. Soil Tillage Res 47:73–81. doi:10.1016/S0167-1987(98)00075-0

Bolzon G, Schrefler BA (2005) Thermal effects in partially saturated soils: a constitutive model. Int J Numer Anal Methods Geomech 29:861–877. doi:10.1002/nag.437

Campanella R, Mitchell J (1968) Influence of temperature variations on soil behavior. J Soil Mech Found 94:709–734

Cekerevac C, Laloui L (2004) Experimental study of thermal effects on the mechanical behaviour of a clay. Int J Numer Anal Methods Geomech 28:209–228. doi:10.1002/nag.332

Cui YJ, Sultan N, Delage P (2000) A thermomechanical model for saturated clays. Can Geotech J 37:607–620. doi:10.1139/t99-111

Delage P, Graham J (1996) Mechanical behaviour of unsaturated soils: understanding the behaviour of unsaturated soils requires reliable conceptual models. In: Proceedings of the 1st international conference on unsaturated soils, Paris, France, September 1995, vol 3. Balkema, A.A., Rotterdam, pp 1223–1256

Elbanna E, Witney B (1987) Cone penetration resistance equation as a function of the clay ratio, soil moisture content and specific weight. J Terramech 24:41–56

Farrell D, Greacen E (1966) Resistance to penetration of fine probes in compressible soil. Aust J Soil Res 4:1–17

Gardner R (1955) Relations of temperature to moisture tension of soil. Soil Sci 79:257–266

Grant S, Salehzadeh A (1996) Calculation of temperature effects on wetting coefficients of porous solids and their capillary pressure functions. Water Resour Res 32:261–270

Haghighi A, Medero G, Woodward P, Laloui L (2011) Effect of temperature on collapse potential of kaolin clay. In: Proc 5th Int Conf on Unsaturated Soils, Barcelona, Spain, 6–8 September 2010, pp 543–548

Hueckel T, Borsetto M (1990) Thermoplasticity of saturated soils and shales: constitutive equations. J Geotech Eng 116:1765–1777

Lingnau BE, Graham J, Yarechewski D et al (1996) Effects of temperature on strength and compressibility of sand-bentonite buffer. Eng Geol 41:103–115. doi:10.1016/0013-7952(95)00028-3

Liu Z, Shi B, Sheng D (2006) A micropenetrometer for detecting structural strength inside soft soils. Geotech Test J 29:1–8

Lloret A, Villar MV (2007) Advances on the knowledge of the thermo-hydro-mechanical behaviour of heavily compacted "FEBEX" bentonite. Phys Chem Earth Parts A/B/C 32:701–715. doi:10.1016/j.pce.2006.03.002

Low HE, Lunne T, Andersen KH et al (2010) Estimation of intact and remoulded undrained shear strengths from penetration tests in soft clays. Géotechnique 60:843–859. doi:10.1680/geot.9.P.017

Lunne T, Eide O, Ruiter J (1976) Correlations between cone resistance and vane shear strength in some Scandinavian soft to medium stiff clays. Can Geotech J 13:430–441

Mitchell J, Soga K (2005) Fundamentals of soil behavior, 3rd edn. Wiley, Hoboken, pp 109–141

Romero E, Gens A, Lloret A (1999) Water permeability, water retention and microstructure of unsaturated compacted Boom clay. Eng Geol 54:117–127. doi:10.1016/S0013-7952(99)00067-8

Romero E, Gens A, Lloret A (2001) Temperature effects on the hydraulic behaviour of an unsaturated clay. Geotech Geol Eng 19:311–332

Romero E, Gens A, Lloret A (2003) Suction effects on a compacted clay under non-isothermal conditions. Géotechnique 53:65–81. doi:10.1680/geot.2003.53.1.65

Romero E, Villar MV, Lloret A (2005) Thermo-hydro-mechanical behaviour of two heavily overconsolidated clays. Eng Geol 81:255–268. doi:10.1016/j.enggeo.2005.06.011

Saix C, Devillers P, El Youssoufi MS (2000) Éléments de couplage thermomécanique dans la consolidation de sols non saturés. Can Geotech J 37:308–317

Seneviratne H, Carter J (1993) A review of models for predicting the thermomechanical behaviour of soft clays. Int J Numer Anal Methods Geomech 17:715–733

Shi B, Liu Z, Cai Y (2005) Development of the super mini-penetrometer and its application. Rock Soil Mech 26:1211–1215

Shin YJ, Kim D (2011) Assessment of undrained shear strength based on Cone Penetration Test (CPT) for clayey soils. KSCE J Civ Eng 15:1161–1166. doi:10.1007/s12205-011-0808-6

Sultan N, Delage P, Cui Y (2002) Temperature effects on the volume change behaviour of Boom clay. Eng Geol 64:135–145. doi:10.1016/S0013-7952(01)00143-0

Tang A-M, Cui Y-J, Barnel N (2008) Thermo-mechanical behaviour of a compacted swelling clay. Géotechnique 58:45–54. doi:10.1680/geot.2008.58.1.45

Tang C-S, Shi B, Zhao L-Z (2010) Interfacial shear strength of fiber reinforced soil. Geotext Geomembr 28:54–62. doi:10.1016/j.geotexmem.2009.10.001

Towhata I, Kuntiwattanaku P, Seko I, Ohishi K (1993) Volume change of clays induced by heating as observed in consolidation tests. Soils Found 33:170–183

Uchaipichat A, Khalili N (2009) Experimental investigation of thermo-hydro-mechanical behaviour of an unsaturated silt. Geotechnique 59:339–353

Villar M, Lloret A (2004) Influence of temperature on the hydro-mechanical behaviour of a compacted bentonite. Appl Clay Sci 26:337–350. doi:10.1016/j.clay.2003.12.026

Wiebe B, Graham J, Tang GX, Dixon D (1998) Influence of pressure, saturation, and temperature on the behaviour of unsaturated sand-bentonite. Can Geotech J 35:194–205. doi:10.1139/t97-093